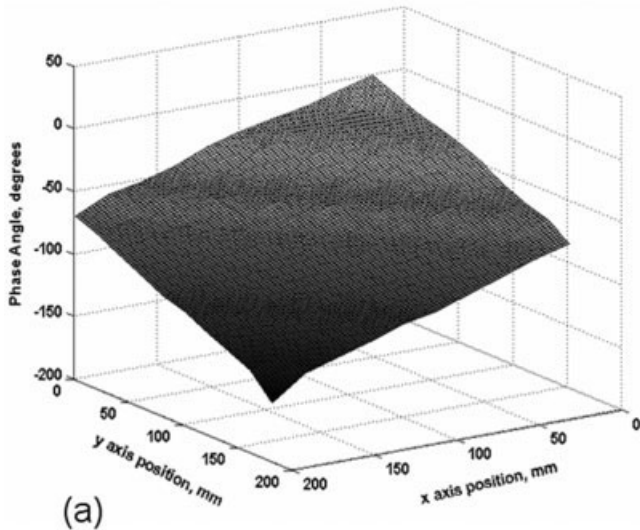
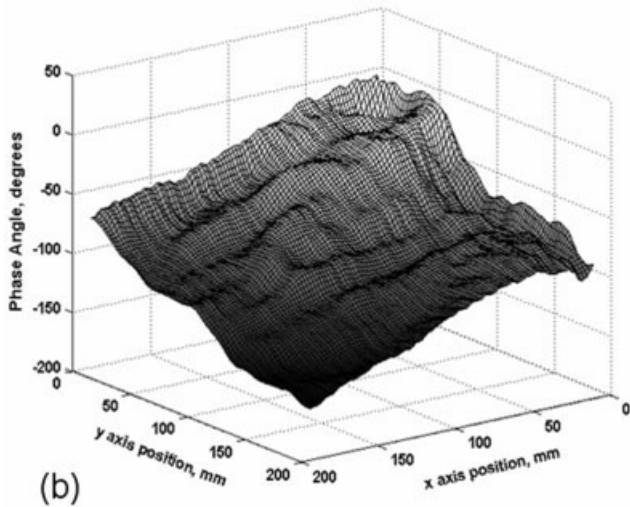


Predicted Phase Response



(a)

Measured Phase Response



(b)

Figure 7 Experimental and predicted results for 2D linear phase ramp DE described in Figure 4(b)

by using larger binary-phase elements. We presented experimental results for two elements operating at 40 GHz that agreed reasonably well with our predictions of expected behavior.

REFERENCES

- N. Nieuborg, A. Kirk, B. Morlion, H. Thienpont, and I. Veretennicoff, Polarization selective diffractive optical elements with an index-matching gap material, *Appl Opt* 36 (1997), 4681–4686.
- L. Pajewski, R. Borghi, and G. Schettini, Design of binary grating with subwavelength features that acts as a polarizing beam splitter, *Appl Opt* 40 (2001), 5898–5905.
- F. Xu, J. Ford, and Y. Fainman, Polarization-selective computer-generated holograms: Design, fabrication, and applications, *Appl Opt* 34 (1995), 256–266.
- M.S. Mirotznik, D.M. Pustai, D.W. Prather, and J.N. Mait, Design of two-dimensional polarization-selective diffractive optical elements with form-birefringent microstructures, *Appl Opt* 43 (2004), 5947–5954.
- P. Lalanne and J. Hugonin, High-order effective-medium theory of subwavelength gratings in classical mounting: Application to volume holograms, *J Opt Soc Am A* 15 (1998), 1843–1851.
- E. Noponen and J. Turunen, Eigenmode method for electromagnetic synthesis of diffractive elements with three-dimensional profiles, *J Opt Soc Am A* 11 (1994), 2494–2502.
- M.G. Moharam, D.A. Pommet, E.B. Grann, and T.K. Gaylord, Stable implementation of the rigorous coupled-wave analysis for surface-relief gratings: Enhanced transmittance matrix approach, *J Opt Soc Am A* 12 (1995), 1077–1084.

© 2007 Wiley Periodicals, Inc.

A BAND-PASS FILTER CONSISTING OF TWO SUBSTRATE INTEGRATED WAVEGUIDE CAVITIES COUPLED BY AN APERTURE ON THEIR COMMON SIDE WALL

R. B. Hwang and C. W. Chang

Communication Engineering Department, National Chiao Tung University, Hsinchu, Taiwan, Republic of China

Received 24 January 2007

ABSTRACT: In this article, we present a substrate-integrated waveguide-based band-pass filter with wide stop-band rejection property. This band-pass filter is made up of two substrate-integrated waveguide cavities, which couple to each other by an aperture on their common waveguide side wall. By using the empirical formula [19] for obtaining the equivalent rectangular waveguide dimensions, the substrate integrated waveguide structure could then be properly approximated by a closed rectangular waveguide. We employed the rigorous mode-matching method to analyze the electromagnetic boundary-value problem of the structure containing multiple discontinuities. In comparison with the conventional end-to-end coupled cavity filters, we found that our new side-wall-coupled cavity filter can suppress the second resonance frequency and therefore, provide a considerably wide rejection band. It is interesting to note that the suppression of the second resonance frequency can be achieved by properly shifting the second cavity in lateral direction. To explore its physical insight, the resonant modes in the substrate integrated waveguide cavities are carefully inspected for realizing the physical picture of wave process taking place in the two cavities system. In addition to the theoretical analysis, we have fabricated the filters and measured their scattering parameters. The good agreement between the theoretical and measured results validates the accuracy of numerical computation, and also shows the promising performance of the proposed filters. © 2007 Wiley Periodicals, Inc.

Microwave Opt Technol Lett 49: 1884–1887, 2007; Published online in Wiley InterScience (www.interscience.wiley.com). DOI 10.1002/mop.22570

Key words: band-pass filter; cavity; substrate integrated waveguide; resonator; periodic structures

1. INTRODUCTION

Waveguide filters have been extensively used in microwave and millimeter wave engineering for many years [1–3]. Because of their high power-handling and high reliability, they were usually applied in deep-space and military radar applications. Recently, the post-wall waveguide technique [4–9], or the substrate integrated waveguide technique [10–19], was developed to fabricate an equivalent rectangular metallic waveguide on a low-loss microwave substrate. Such a class of waveguides has been proved [18] to be able to preserve the well-known advantages of conventional closed rectangular waveguide, such as high-Q factor. Be-

sides, the substrate integrated waveguide is based on printed circuit-board fabrication process; therefore, it is easy to be integrated with the microstrip, coplanar waveguide, or the other planar circuits, to design a microwave/mm-wave sub-system. In addition to the substrate integrated waveguide, the cavity based on the substrate integrated waveguide technology was also well developed [19]. The novel substrate integrated waveguide-cavity filter with defected ground structure was investigated to provide a high stop-band rejection and low insertion loss. The electromagnetic band-gap structures, which reflect the incident wave in their stop-band region, were developed to serve as a waveguide wall for cavity-filter design [20–24].

Besides, the theoretical investigation concerning the guided-wave and leaky-wave characteristics of substrate-integrated waveguide was also treated using numerical multimode calibration procedure combined with the finite-element method [18]. The more accurate empirical formula for determining the equivalent rectangular waveguide-width was developed to provide a valuable design criterion for implementing substrate integrated waveguide [18].

In this article, we designed a band-pass filter using two coupled substrate integrated waveguide-based cavities, which are coupling to each other by an aperture on their common sidewall. By following the design criterion and empirical formula [18], we could have the equivalent closed rectangular waveguide structure parameters. Moreover, the rigorous mode-matching method is employed to convert the 2D electromagnetic boundary-value problem into a transmission-line network including transformer-bank-like input-output relation at the discontinuity. The transmission and reflection characteristics and electromagnetic fields distribution, as well as the substrate integrated waveguide cavities were determined. As is well known for the conventional end-to-end coupled-cavity filter, the second resonant mode provides an extra pass-band. For some practical application, the second pass-band is undesired. To have a band-pass filter with high rejection for the second pass-band, we have offset the second cavity to reduce the aperture coupling. We have fabricated and measured the band-pass filter for verifying the design concept. The good agreement between the measured and calculated results validates the design concept and theoretical analysis model. Besides, the physical mechanism of high stop-band rejection for the second resonant mode was clearly interpreted by inspecting theoretically the contour map of the electric field combined with the simple coupled-mode theory.

2. DESCRIPTION OF THE PROBLEM

Figure 1(a) depicts a conventional end-to-end coupled-cavities filter, where the cavity was made by post-wall (or via-hole) waveguide techniques. Such a type of cavity filter has been developed and applied in microwave system [19]. In this article, we developed a cavity filter, shown in Figures 1(b) and 1(c), consisting of two post-wall-based cavities couple to each other through an aperture on their common waveguide side wall. Each of the waveguide connects with a microstrip line with taper at its end as shown in Figure 1(c). The widths of the two waveguides are h_1 and h_2 , respectively. The widths of the inductive irises in the input and output waveguide are, a_1 and a_2 , respectively. The width of the coupling aperture on the common sidewall of the two waveguides is w . The distances from the inductive irises to the front end of the coupling aperture are l_1 and l_2 , respectively, in the input and output waveguide. The distance from the short circuit board to the aperture are designated as l_3 and l_4 in the two waveguides. The waveguide wall is implemented by placing periodic metallic via-holes with considerably small distance between adjacent holes. To

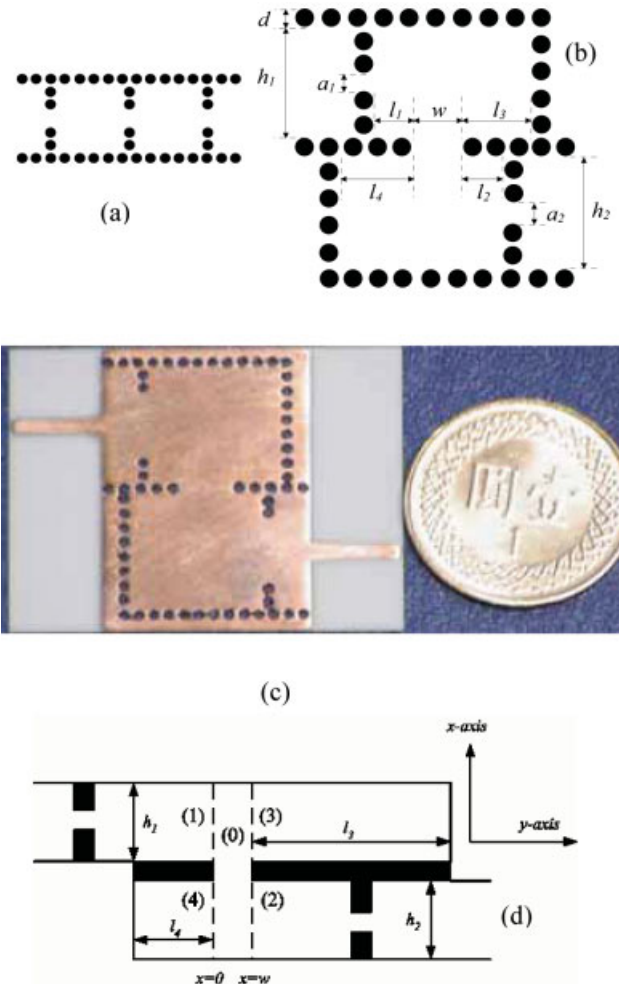


Figure 1 Structure configuration of the substrate-integrated waveguide cavity band-pass filters; (a) conventional end-to-end coupled cavity filter, and (b) side-wall-coupled band-pass filter developed in this paper, (c) circuit topology, and (d) equivalent closed. [Color figure can be viewed in the online issue, which is available at www.interscience.wiley.com]

maintain the waves guided in the waveguide and simultaneously reduce the power leakage, we have followed the criterion reported in the literature [18, 19] to design the substrate integrated waveguide.

3. METHOD OF ANALYSIS

There are many numerical methods well developed for resolving the electric and magnetic fields in the substrate-integrated waveguide. To mention a few, the finite-difference frequency-domain algorithm incorporating the perfect matched layer was developed [19] to discretize the continuous spectrum, and thus the resonance frequency and Q-factor can be obtained by solving a standard matrix eigen-value problem [19]. The finite-element method was also developed to analyze the guided-wave and leaky-wave characteristics of a substrate-integrated waveguide [18]. In this article, we employed the rigorous mode-matching method to deal with the electromagnetic boundary-value problem. First, for simplifying the mathematical analysis, we have used the accurate empirical equation for determining the equivalent-rectangular waveguide-width, w_{eff} , which is given as follow

$$w_{\text{eff}} = w - 1.08(d^2/s) + 0.1(d^2/w). \quad (1)$$

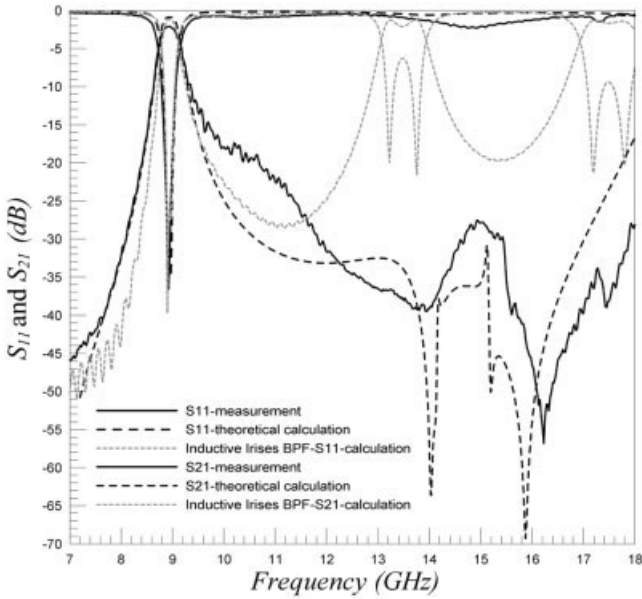


Figure 2 Insertion- and return- loss of the band-passfilter; the geometric parameters are: $h_1 = h_2 = 11$ mm, $l_1 = l_2 = 2.5$, $l_3 = l_4 = 4.12$ mm, $w = 4.3$ mm, $t_{g1} = t_{g2} = 1$ mm, $a_1 = a_2 = 6.2$ mm, $t_m = 1$ mm

where d and s are the diameter and the period of the metallic via-holes, and w is the distance between two via-hole walls (center-to-center). As indicated in [18], when s/d is smaller than three and d/w is smaller than $1/5$, the empirical formula is very accurate. We followed the guideline and criterion given previously to design the waveguide; therefore, the equivalent rectangular waveguide can be determined to model the via-holes waveguide. Furthermore, because that the thickness of the substrate is much smaller compared with the width and length, there exists three field components, i.e., E_z , H_x , and H_y . The E_z component is assumed to be invariant along the z -axis. Therefore, the problem can be simplified to a two-dimensional (2D) boundary-value problem. The mode-matching method was well developed and widely applied in solving the electromagnetic problem with canonical structure, such as rectangular and circular cylindrical waveguides, because the eigen-mode has close-form solution in those structures. Since the structure under consideration consists of many simple rectangular waveguides and discontinuity structures, the mode-matching method was then used to deal with electromagnetic field problem. In the following section, we will briefly introduce the mathematical procedure for solving the electromagnetic fields in the structure; however, the detailed mathematical derivation and procedure could be found in the literature [25].

4. NUMERICAL AND EXPERIMENTAL RESULTS

Based on the mathematical formulation mentioned earlier, we have developed a computer program to calculate the electric and magnetic fields distribution in the structure, as well as the scattering parameters, such as return- and insertion- loss at the input and output ports, respectively. Although not shown here, we have carefully examined the numerical convergence against the number of waveguide modes employed, and the field continuity at the discontinuities, as well. In addition to the numerical simulation, we have carried out the experimental studies by fabricating the printed waveguide on the microwave substrate Rogers RO4003 with thickness 20 mil. The metallic via-hole, connecting the top and bottom metal plates, was implemented by electroplating technique to

ensure a good electrical performance. The period of via holes is 1.4 mm. The distance between two adjacent via-holes is 0.4 mm. The S-parameters were measured using vector network analyzer HP-8722D, and the universal test fixture Anritsu3680K employed for reducing the loss due to SMA connector.

Figure 2 depicts the return loss and insertion loss of the band-pass filter, shown in Figures 1(b) and 1(c), developed in this article. Besides, substrate-integrated-waveguide-based end-to-end coupled cavity filter, shown in Figure 1(a), was demonstrated to compare their performance. The black and long dashed lines in this figure represent the calculated return- and insertion- loss, while the solid lines stand for the measured ones. The gray and short dashed lines are the calculated return- and insertion- loss of the end-to-end coupled band-pass filter. In this example, the windows of the inductive irises are the same for the two band-pass filters. Besides, all the cavities share the same dimensions.

From this figure, it is apparently to see a good agreement between the calculated and measured S-parameters. This may confirm the accuracy of the theoretical analysis model developed in this article. It is noted that in this figure the end-to-end coupled cavity filter has a second pass band around 13.5 GHz. On the contrary, the band-pass filter developed in this article can suppress this resonant mode. In fact, the pass-band frequency can be roughly estimated by the resonance frequency of the waveguide cavity; for instance, the resonance wavelength of the cavity resonant modes TM_{mn0} is given below

$$\lambda_{mn} = 2 \sqrt{\epsilon_s} / \sqrt{(m/a)^2 + (n/b)^2}. \quad (2)$$

the indices m , n , and 0 denote the mode number along the width-, length-, and thickness-direction, respectively. Since the thickness of the waveguide is much smaller compared with the width and length, the index number is set to zero. It is obvious to see that the pass band around 9 GHz corresponds to the TM_{110} resonant mode, while the second pass band, taking place around 13.5 GHz corresponding to that of TM_{120} resonant mode. However, the second pass band disappears in the sidewall aperture coupling band-pass filter case. In the following numerical example, we will explain this phenomenon by investigating the electric field distribution in the two coupled cavities.

Figure 3 shows the contour map for the electric field distribution in the two cavities. The polarization of the electric field drawn in this figure is along the z -direction. In Figure 3(a), the operation frequency is 9.0 GHz, locating in the first pass-band region. From

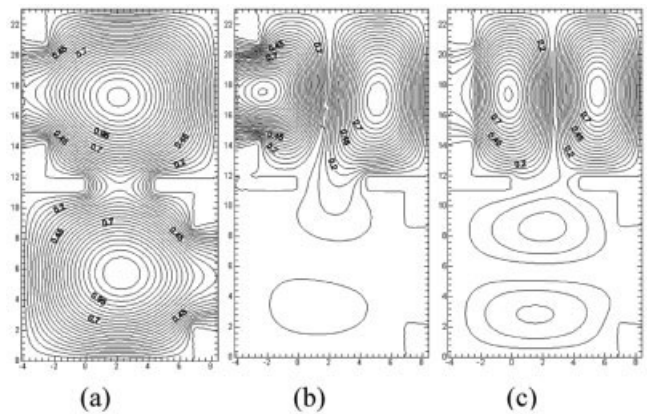


Figure 3 Contour map for the electric field (E_z component) in the two cavities: (a) 9.0 GHz, (b) 13.4 GHz and (c) 15 GHz, respectively

this figure, we may clearly see that the resonant mode in both cavities is TM_{110} ; the maximum field strength takes place around the middle of the cavity. Since the aperture is opened at the position near the maximum electric field, the energy can be significantly coupled from the first cavity to the second one. Conversely, in the Figure 3(b), the frequency 13.4 GHz, corresponds to the resonant mode, TM_{120} , thus the electric field distribution along the y -axis could be roughly predicted by $\sin(2\pi y/(l_1 + l_3 + w))$. Around the center region; that is $y \approx 0.5/(l_1 + l_3 + w)$, the electric field is almost vanishing. Therefore, the electric field coupling through the aperture is inconsiderable, as shown in Figure 3(c). Notice that in Figure 3(c), the two cavities almost have the same dimensions along the x and y direction, thus the TM_{120} and TM_{210} resonant modes almost share the same resonant frequency, 15 GHz. The TM_{120} mode, in the first cavity, is coupling to the TM_{210} mode in the second cavity; however, because of the minimum field strength occurring in the middle along width direction, the output signal is insignificant. It may conclude the phenomenon of considerable suppression for the undesired resonant frequencies, as illustrated in Figure 2.

5. CONCLUSION

In this article, a band-pass filter made up of two substrate-integrated-waveguide-based cavities coupled by an aperture on their common side wall was investigated theoretically and experimentally. The theoretical analysis using the rigorous mode-matching method incorporating the transmission-line representation was employed to calculate the reflection and transmission characteristics, as well as the electric fields distribution. It is interesting to note that by shifting the position of the second cavity in the lateral direction, the second resonant mode is greatly suppressed, and thus provide a high stop-band rejection for this harmonic. This concept was verified by theoretically inspecting the electric fields distribution in the two-cavity system. The good agreement between the calculated and measured results confirms the theoretical formation. Besides, such a band-pass filter design can provide a low insertion loss around 9 GHz, and a high rejection for the second pass-band. It may be a promising design in realizing a low-cost printed circuit based waveguide filter design.

ACKNOWLEDGMENT

This research work is sponsored by National Science Council.

REFERENCES

1. A.E. Atia and A.E. Williams, Narrow-bandpass waveguide filters, *IEEE Trans Microwave Theory Tech MTT-20* (1972), 258–265.
2. R.J. Cameron, General coupling matrix synthesis methods for Chebyshev filtering functions, *IEEE Trans Microwave Theory Tech* 47 (1999), 433–442.
3. R. Levy, R.V. Snyder, and G. Matthaei, Design of microwave filters, *IEEE Trans Microwave Theory Tech* 50 (2002), 783–793.
4. H. Uchimura and T. Takenoshita, Development of a laminated-waveguide, *IEEE Trans Microwave Theory Tech* 46 (1998), 2438–2443.
5. J. Hirokawa and M. Ando, Single-layer feed waveguide consisting of posts for plane TEM wave excitation in parallel plates, *IEEE Trans Antennas Propag* 46 (1998), 625–630.
6. J. Hirokawa and M. Ando, Efficiency of 76-GHz post-wall waveguide-fed parallel-plate slot arrays, *IEEE Trans Antennas Propag* 48 (2000), 1742–1745.
7. Y. Rong, K.A. Zaki, J. Gipprich, M. Hageman, and D. Stevens, LTCC wide-band ridge-waveguide bandpass filters, *IEEE Trans Microwave Theory Tech* 47 (1999), 1836–1840.
8. Y. Rong, K.A. Zaki, M. Hageman, D. Stevens, and J. Gipprich, Low temperature cofired ceramic (LTCC) ridge waveguide bandpass chip filters, *IEEE Trans Microwave Theory Tech* 47 (1999), 2317–2324.
9. A. Zeid and H. Baudrand, Electromagnetic scattering by metallic holes and its applications in microwave circuit design, *IEEE Trans Microwave Theory Tech* 50 (2002), 1198–1206.
10. D. Deslandes and K. Wu, Single-substrate integration technique of planar circuits and waveguide filters, *IEEE Trans Microwave Theory Tech* 51 (2003), 593–596.
11. D. Deslandes and K. Wu, Integrated microstrip and rectangular-waveguide in planar form, *IEEE Microwave Wireless Compon Lett* 11 (2001), 68–70.
12. Y. Cassivi, L. Perregrini, P. Arcioni, M. Bressan, K. Wu, and G. Conciauro, Dispersion characteristics of substrate integrated rectangular waveguide, *IEEE Microwave Wireless Compon Lett* 12 (2002), 333–335.
13. Y. Cassivi and K. Wu, Low cost microwave oscillator using substrate integrated waveguide cavity, *IEEE Microwave Wireless Compon Lett* 13 (2003), 48–50.
14. F. Xu, Y.L. Zhang, W. Hong, K. Wu, and T.J. Cui, Finite-difference frequency-domain algorithm for modeling guided-wave properties of substrate integrated waveguide, *IEEE Trans Microwave Theory Tech* 51 (2003), 2221–2227.
15. H. Li, W. Hong, T.J. Cui, K. Wu, Y.L. Zhang, and L. Yan, Propagation characteristics of substrate integrated waveguides based on LTCC, In *IEEE MTT-S International Microwave Symposium Digest*, Philadelphia, PA, 2003, pp. 2045–2048.
16. Y. Huang, K.L. Wu, and M. Ehlert, An integrated LTCC laminated waveguide-to-microstrip line T-junction, *IEEE Microwave Wireless Compon Lett* 13 (2003), 338–339.
17. Z.C. Hao, W. Hong, X.P. Chen, J.X. Chen, K. Wu, and T.J. Cui, Multilayered substrate integrated waveguide (M SUBSTRATE INTEGRATED WAVEGUIDE) elliptic filter, *IEEE Microwave Wireless Compon Lett* 15 (2005), 95–97.
18. F. Xu and K. Wu, Guided-wave and leakage characteristics of substrate integrated waveguide, *IEEE Trans Microwave Theory Tech* 53 (2005), 66–73.
19. Y.L. Zhang, W. Hong, K. Wu, J.X. Chen, and H.J. Tang, Novel substrate integrated waveguide cavity filter with defected ground structure, *IEEE Trans Microwave Theory Tech* 53 (2005), 1280–1287.
20. J. Papapolymerou, J. Cheng, J. East, and L. Katehi, A micromachined-high-QX-band resonator, *IEEE Microwave Guided Wave Lett* 7 (1997), 168–170.
21. M.J. Hill, R.W. Ziolkowski, and J. Papapolymerou, Simulated and measured results from a duroid-based planar MBG cavity resonator filter, *IEEE Microwave Guided Wave Lett* 10 (2000), 528–530.
22. W.J. Chappell, M.P. Little, and L.P.B. Katehi, High isolation, planar filters using EBG substrates, *IEEE Microwave Wireless Compon Lett* 11 (2001), 246–248.
23. H.J. Hsu, M.J. Hill, R.W. Ziolkowski, and J. Papapolymerou, Aduroid-based planar EBG cavity resonator filter with improved quality factor, *IEEE Antennas Wireless Propag Lett* 1 (2002), 67–70.
24. H.J. Hsu, M.J. Hill, J. Papapolymerou, and R.W. Ziolkowski, A planar X-band electromagnetic bandgap (EBG) 3-pole filter, *IEEE Microwave Wireless Compon Lett* 12 (2002), 255–257.
25. N. Marcuvitz, *Waveguide handbook*, McGraw-Hill, New York, NY, 1951.

© 2007 Wiley Periodicals, Inc.